THE JOURNAL OF BIOLOGICAL CHEMISTRY
Vol. 278, No. 48, Issue of November 28, pp. 47987–47996, 2003
Printed in U.S.A.

Structural Rearrangements of the 10–23 DNAzyme to β3 Integrin Subunit mRNA Induced by Cations and Their Relations to the Catalytic Activity*

Received for publication, January 16, 2003, and in revised form, July 22, 2003
Published, JBC Papers in Press, September 2, 2003, DOI 10.1074/jbc.M300504200

Marcin Cieslak‡, Jacek Szymanski§, Ryszard W. Adamiak¶, and Czeslaw S. Cierniewski§‖**

From the Centers for ‡Molecular and Macromolecular Studies and ‖Medical Biology and Microbiology, Polish Academy of Sciences, §Department of Molecular and Medical Biophysics, Medical University of Lodz, 92-215 Lodz, Poland and ¶Institute of Bioorganic Chemistry, Polish Academy of Sciences, 61-704 Poznan, Poland

The intracellular ability of the "10–23" DNAzyme to efficiently inhibit expression of targeted proteins has been evidenced by *in vitro* and *in vivo* studies. However, standard conditions for kinetic measurements of the DNAzyme catalytic activity *in vitro* include 25 mM Mg^{2+}, a concentration that is very unlikely to be achieved intracellularly. To study this discrepancy, we analyzed the folding transitions of the 10–23 DNAzyme induced by Mg^{2+}. For this purpose, spectroscopic analyzes such as fluorescence resonance energy transfer, fluorescence anisotropy, circular dichroism, and surface plasmon resonance measurements were performed. The global geometry of the DNAzyme in the absence of added Mg^{2+} seems to be essentially extended, has no catalytic activity, and shows a very low binding affinity to its RNA substrate. The folding of the DNAzyme induced by binding of Mg^{2+} may occur in several distinct stages. The first stage, observed at 0.5 mM Mg^{2+}, corresponds to the formation of a compact structure with limited binding properties and without catalytic activity. Then, at 5 mM Mg^{2+}, flanking arms are projected at right position and angles to bind RNA. In such a state, DNAzyme shows substantial binding to its substrate and significant catalytic activity. Finally, the transition occurring at 15 mM Mg^{2+} leads to the formation of the catalytic domain, and DNAzyme shows high binding affinity toward substrate and efficient catalytic activity. Under conditions simulating intracellular conditions, the DNAzyme was only partially folded, did not bind to its substrate, and showed only residual catalytic activity, suggesting that it may be inactive in the transfected cells and behave like antisense oligodeoxynucleotide.

The typical DNAzyme,[1] known as the "10–23" model, has tremendous potential in gene suppression for both target validation and therapeutic applications (1). It is capable of cleaving single-stranded RNA at specific sites under simulated physiological conditions and can be used to control even complex biological processes such as tumor angiogenesis. For example, DNAzymes to β1 and β3 mRNA reduced expression of targeted integrin subunits in endothelial cells and blocked proliferation, migration, and network formation in a fibrin and Matrigel™ matrix (2). In a cell culture system, a 10–23 deoxyribozyme designed against 12-lipoxygenase mRNA specifically down-regulated expression of this protein and its metabolites, which are known to play a crucial role in tumor angiogenesis (3). Similarly, the DNAzyme to VEGFR2 mRNA cleaved its substrate efficiently and inhibited the proliferation of endothelial cells with a concomitant reduction of VEGFR2 mRNA and blocked tumor growth *in vivo* (4).

The origins of the DNAzyme catalytic activity are not yet fully understood, but the observed rate enhancements probably are generated by a number of factors, including metal ion and nucleobase catalysis and local stereochemical effects. The 10–23 DNAzyme has been developed using an *in vitro* selection strategy on the basis of its ability to cleave RNA in the presence of Mg^{2+} (1). It has a catalytic domain of 15 highly conserved deoxyribonucleotides flanked by two substrate-recognition domains and can cleave effectively between any unpaired purine and pyrimidine of mRNA transcripts. Like many other enzymes catalyzing phosphoryl-transfer reactions, it is recognized as a metalloenzyme requiring divalent metal, preferentially Mg^{2+} ions, for catalytic activity. Divalent cations play a crucial role in these mechanisms, as evidenced by a number of observations. For example, addition of La^{3+} to the Mg^{2+}-background reaction mixture inhibited the DNAzyme-catalyzed reactions, suggesting the replacement of catalytically and/or structurally important Mg^{2+} by La^{3+} (5). The function of divalent metal cations in DNAzyme activity is very complex and includes (i) stabilization of the transition state of reaction. The divalent metal cation dependence of the enzyme was described as being the evidence supporting a chemical mechanism involving metal-assisted deprotonation of the 2′-hydroxyl located adjacent to the cleavage site (6). It also includes (ii) neutralization of negative charges of phosphate groups, thus facilitating DNA-RNA interactions. High resolution x-ray crystal structures of Mg^{2+} and Ca^{2+} salts of the model B-DNA decamers CCAACGTTGG and CCAGCGCTGG revealed sequence-specific binding of Mg^{2+} and Ca^{2+} to the major and minor grooves of DNA, as well as nonspecific binding to backbone phosphate oxygen atoms. This accounts for the neutralization of between 50 and 100% of the negative charges of phosphate groups (7). (iii) Some of these bound cations may also play a purely structural role by inducing proper folding of the DNAzyme molecule, thus helping to organize the enzyme into its active conformation. There are several reports showing that Mg^{2+} helps to stabilize different types of double-stranded DNA structures (8,

* This work was supported by Grant Z-KBN 004/PO4/98 from the Polish Committee for Scientific Research. The costs of publication of this article were defrayed in part by the payment of page charges. This article must therefore be hereby marked "*advertisement*" in accordance with 18 U.S.C. Section 1734 solely to indicate this fact.

** To whom correspondence should be addressed: Dept. of Molecular and Medical Biophysics, Medical University of Lodz, 6/8 Mazowiecka Street, 92–215 Lodz, Poland. Tel.: 48-42-6783393; Fax: 48-42-6789433; E-mail: cciern@zdn.am.lodz.pl.

[1] The abbreviations used are: DNAzyme, DNA enzyme suitable for the sequence-specific cleavage of RNA; FRET, fluorescence resonance energy transfer; HPLC, high pressure liquid chromatography; HUVEC, human umbilical vein endothelial cell.

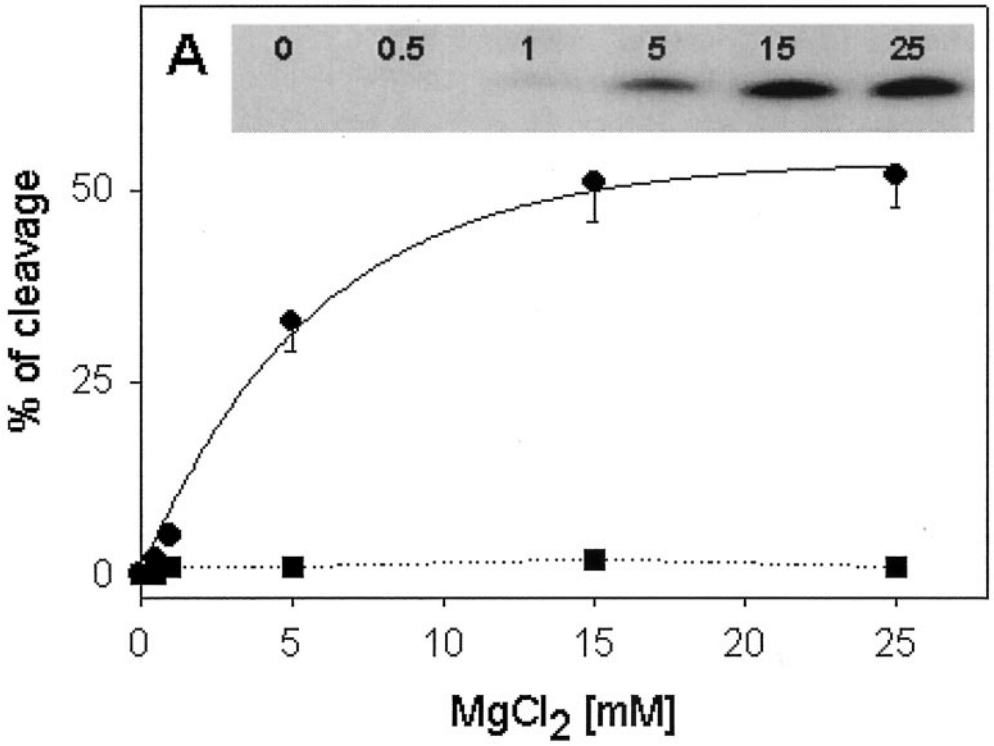

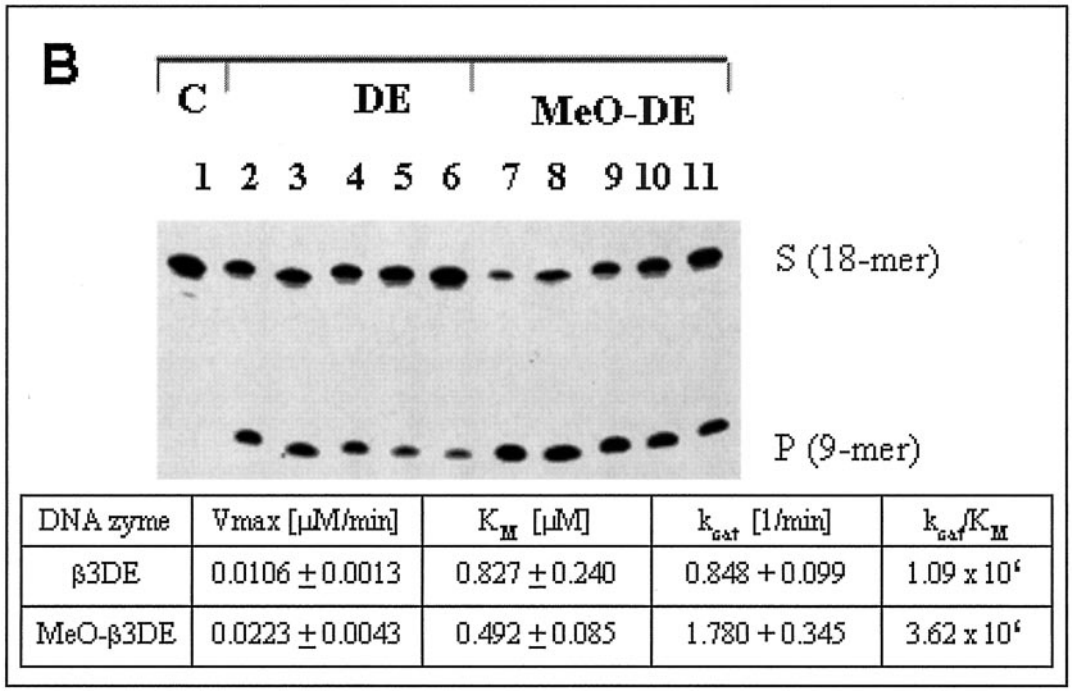

DNA zyme	Vmax [μM/min]	K_M [μM]	k_{cat} [1/min]	k_{cat}/K_M
β3DE	0.0106 ± 0.0013	0.827 ± 0.240	0.848 + 0.099	1.09 x 10^4
MeO-β3DE	0.0223 ± 0.0043	0.492 ± 0.085	1.780 + 0.345	3.62 x 10^4

FIG. 1. **Cleavage of β3 integrin subunit mRNA substrate by DNAzymes *in vitro*.** *A*, the effect of Mg^{2+} concentration on enzymatic activity of DNAzymes. MeO-β3DE$_{(15)}$ (●–●) and its mutant MeO-β3DE$_{(11)}$ (■–■) were incubated with the RNA substrate (molar ratio, 1:80) for 10 min in the presence of increasing concentrations of Mg^{2+} ranging from 0 to 25 mM. The cleavage reaction was stopped by the addition of 0.5 M EDTA, and the products were separated by electrophoresis in 20% polyacrylamide gels under denaturing conditions. Relative amounts of cleavage products (*% of cleavage*) are plotted *versus* Mg^{2+} concentration (*$MgCl_2$[mM]*). *Inset*, autoradiogram of the gel showing the cleavage product obtained at different Mg^{2+} concentrations (0–25 mM). *B*, catalytic activity of β3DE and MeO-β3DE. In these experiments, aliquots of the ^{32}P-labeled mRNA substrate were incubated with DNAzymes. β3DE and MeO-β3DE were used at a molar ratio (substrate:enzyme) ranging from 5:1 to 80:1 for up to 60 min at 37 °C. The cleavage products obtained after a 10-min incubation of ^{32}P-labeled mRNA substrate are shown alone (*lane 1*) or with DNAzymes (β3DE, MeO-β3DE) mixed at the ratio 5:1 (*lanes 2* and *7*), 10:1 (*lanes 3* and *8*), 20:1 (*lanes 4* and *9*), 40:1 (*lanes 5* and *10*), and 80:1 (*lanes 6* and *11*). DNAzymes were used at the concentration of 0.025 μM. Reactions were carried out in 50 mM Tris, pH 8.0, containing 15 mM $MgCl_2$, 0.01% SDS. Amounts of the product were evaluated by a PhosphorImager (Amersham Biosciences) and used to calculate kinetic parameters. They were determined in multiple turnover reactions and represent a mean of three independent experiments.

9) and can induce bending or enhance curvature in DNA (10). Furthermore, Mg^{2+} and other divalent cations enhance end-to-end DNA interactions, particularly in the case of fragments with self-complementary ends (11). These structural effects of cations may be even more profound in a single-stranded and flexible DNAzyme molecule.

Mg^{2+}-dependent cleavage has special relevance to biology because it is compatible with intracellular conditions, raising the possibility that DNA enzymes might be made to operate *in vivo* (12). However, at the present time, it is hard to explain their intracellular catalytic activity, keeping in mind the catalytic dependence upon high concentrations of Mg^{2+}, which is unlikely to be achieved in cytoplasm. To address the question of their intracellular catalytic activity, we attempted to correlate changes in the catalytic activity and configuration of the DNAzyme induced by gradually bound Mg^{2+}. To characterize structural changes in the DNAzyme, we performed fluorescence resonance energy transfer (FRET) analysis, which allowed us to monitor general folding of the molecule based on the measurements of distances between fluorophores linked to 5′ and 3′ side bases, and surface plasmon resonance analysis of the DNAzyme binding to its RNA substrate. Structural changes induced by cations in DNAzymes were also monitored by circular dichroism and fluorescence anisotropy analysis.

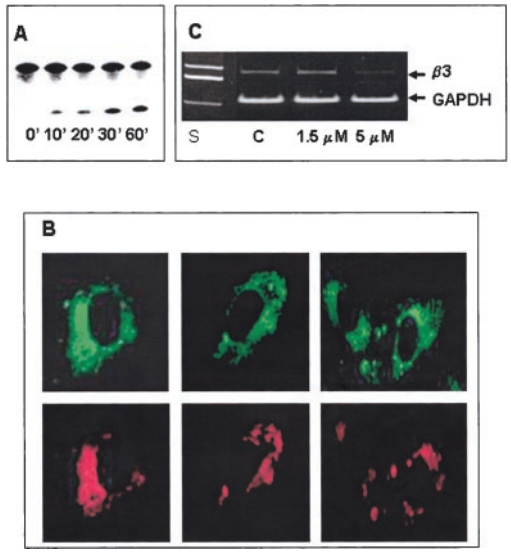

FIG. 2. **Biological activity of Fluo-MeO-β3DE-Rhod.** *A*, DNAzyme activity of the fluorophore-labeled construct identical to that used for the FRET analysis. The cleavage activity was examined after incubation of Fluo-MeO-β3DE-Rhod with a 20-fold excess of 5′-^{32}P-labeled RNA substrate in the presence of 15 mM $MgCl_2$ at 37 °C. A sample was removed at different time points (*lanes 1-5*). *B*, the fluorescence image of endothelial cells treated with Fluo-MeO-β3DE-Rhod. Endothelial cells, exposed to 0.5 μM of the fluorophore-labeled construct for 24 h at 37 °C and processed as described under "Experimental Procedures," were analyzed by confocal fluorescence microscopy. The punctate fluorescence distribution within the cytoplasm was detected by monitoring both fluorescein and rhodamine attached to DNAzyme. *C*, the reduced expression of β3 mRNA in HUVECs treated with MeO-β3DE when compared with unchanged expression in untreated cells. β3 mRNA was evaluated by relative quantitative reverse transcriptase-PCR using glyceraldehyde-3-phosphate dehydrogenase mRNA as an intrinsic control.

EXPERIMENTAL PROCEDURES

Synthesis of DNAzyme to β3 mRNA—DNAzyme was chemically synthesized on a solid support using an ABI-394 DNA synthesizer, as described previously (13). This particular DNA sequence (5′-GAGTCCCATA$g_1g_2c_3t_4a_5g_6c_7t_8a_9c_{10}a_{11}a_{12}c_{13}g_{14}a_{15}$AAGACTTGAG-3′) was used previously to analyze the enzymatic activity, specificity, exonuclease resistance, and ability to inhibit expression of β3 integrins in endothelial cells (2). For BIAcore experiments, the inactive DNAzyme, $\beta3DE_{(15)In}$, with a single substitution ($G^6 \rightarrow A$) in the reactive loop and antisense oligodeoxynucleotide β3(1245–1265) containing both flanking arms of the β3DE (5′-GAGTCCCATACAAGACTTGAG-3′) were synthesized. Two analogues of $\beta3DE_{(15)In}$ and β3(1245–1265) were produced as well, which contained the modified oligonucleotides such as phosphorothioates or 2′-*O*-methyl-substituted residues introduced at both 5′ and 3′ sides. Hence, S-$\beta3DE_{(15)in}$ and S-β3(1245–1265) have two phosphorothioate substitutions, whereas MeO-$\beta3DE_{(15)in}$ and MeO-β3(1245–1265) contain two 2′-*O*-methyl-substituted residues at both their 5′ and 3′ sides, respectively. An additional mutated DNAzyme (MeO-$\beta3DE_{(11)}$) with a downsized catalytic loop of a deoxyribozyme from 15-mer to 11-mer (5′-GAGTCCCA-TA$g_1g_2c_3t_4a_9c_{10}a_{11}a_{12}c_{13}g_{14}a_{15}$AAGACTTGAG-3′) was synthesized and used as a control. DNAzymes with the 11-mer catalytic loop were described to be Ca^{2+}-dependent deoxyribozymes and showed significantly reduced binding affinities and catalytic activities in the pres-

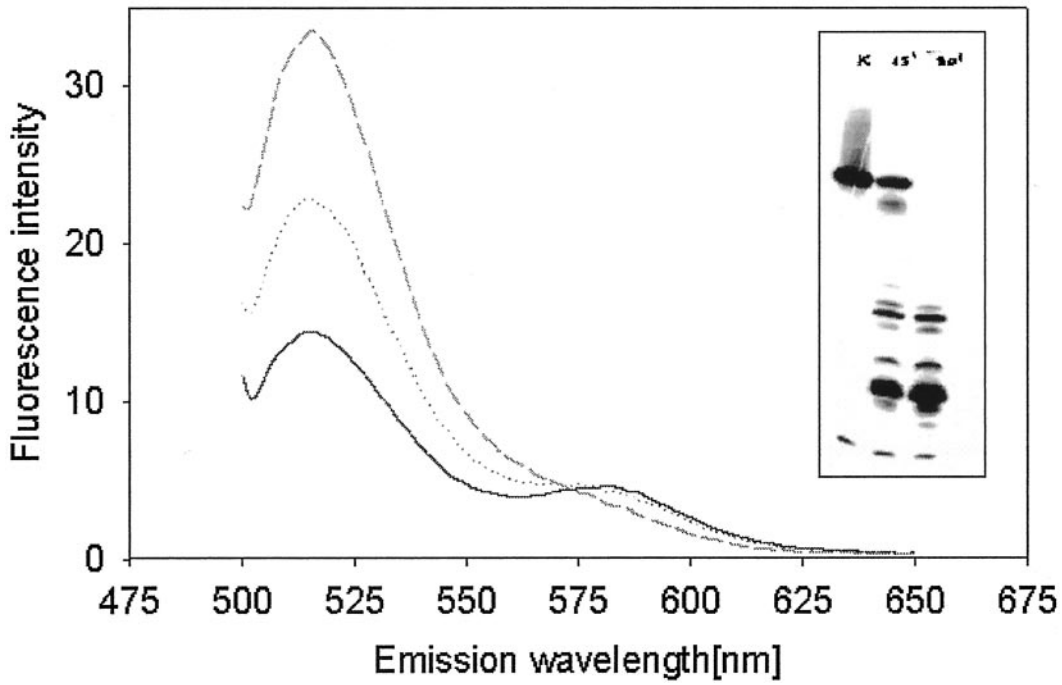

FIG. 3. **Fluorescence resonance energy transfer between fluorescein and rhodamine attached to MeO-β3DE at 3′ and 5′ ends, respectively.** Fluo-MeO-β3DE-Rhod (40 nM) had two peaks at 520 nm and 580 nm upon excitation at 494 nm. *Inset*, autoradiogram of a gel after electrophoresis of the Fluo-MeO-β3DE-Rhod digested with endonuclease from *S. marcescens*. Degradation of the fluorophore-labeled DNAzyme resulted in a significant increase in fluorescence intensity at 520 nm and a disappearance of the 580 nm maximum.

ence of Mg^{2+} (14). All deoxyoligonucleotides were purified by HPLC and ion exchange chromatography (to 98%), and their purity was checked by PAGE under denaturing conditions.

The doubly labeled β3 DNAzymes with the 15-mer and 11-mer catalytic loops were synthesized by the solid-state phosphoramidite approach on an ABI 392 synthesizer, starting from fluorescein CPG support (CPG, Inc.). The 2′-*O*-Me RNA cyanoethyl phosphoramidites (Glen Research) were used for introduction of 2′-*O*-Me nucleotide units flanking the sequence from the 3′ and 5′ ends. The synthesis was terminated with the addition of rhodamine cyanoethyl phosphoramidite (CPG, Inc.). Oligonucleotides were cleaved from the solid support and deprotected by brief (4 h at 55 °C) treatment with 30% ammonia. Pure product was isolated by preparative HPLC on a Hamilton PRP1 column. The peak fractions were evaporated to dryness, redissolved in water, and then ethanol-precipitated.

The synthetic, biotinylated (at the 3′ end) 21-mer RNA (biotin-CUCAGGGUAUGUUCUGAACUC) used in BIAcore experiments was purchased from Bionovo (Poland). Its sequence corresponded to the 1245–1265 fragment of β3 mRNA. After synthesis, the product was purified by HPLC and its purity was checked by PAGE.

Preparation of Target RNA Substrates and Kinetic Analysis—Aliquots of RNA substrates (20 μl, 5 μM) dissolved in a T4 polynucleotide kinase buffer were mixed with [γ-^{32}P]ATP (2 μl, 20 μCi) and T4 polynucleotide kinase (3 units). Reaction was carried out for an h at 37 °C. All reported kinetic values were determined in multiple turnover reactions. V_{max} and K_m values were determined from the *y* intercept and slope, respectively, of the best-fit line to a Lineweaver-Burke plot of 1/V *versus* 1/[S]. Reactions (10 min at 37 °C; total volume = 20 μl) were carried out in 50 mM Tris, pH 8.0, containing 15 mM $MgCl_2$, 0.01% SDS, DNAzyme (0.0125 μM) with the radiolabeled RNA substrate used in a wide range of concentrations. The cleavage reaction was stopped by the addition of 5 μl of 0.5 M EDTA, and the products were separated by electrophoresis in 20% polyacrylamide gels under denaturing conditions. Amounts of the product were evaluated by use of a PhosphorImager (Amersham Biosciences).

Cell Culture—Human umbilical vein endothelial cells (HUVEC) were isolated from freshly collected umbilical cords by collagenase treatment (15, 16). Cells were grown in gelatin-coated 75-cm^2 tissue culture flasks and were maintained at confluence in RPMI 1640 medium supplemented with streptomycin (100 μg/ml), penicillin (100 units/ml), fungizone (2.5 mg/ml), heparin (90 μg/ml), L-glutamine (1 mM), sodium bicarbonate (2 mg/ml), 20% fetal bovine serum, and epidermal growth factor (40 ng/ml) at 37 °C in a humidified 5% CO_2 atmosphere. Primary cultures were harvested at confluence with trypsin/EDTA and transferred into gelatin-coated dishes. For the experiments, confluent cultures were used at the second passage.

For microscopic examination, cells were plated at a density of 5×10^4 cells/well on Thermanox cover-slips in 8-well tissue culture chamber slides (NUNC) with detachable chambered upper structures. Before performance of assays, the serum-containing medium was changed to a serum-free medium (Opti-MEM). The cultures were gently rinsed three times with the medium and preincubated with fluorophore-labeled MeOβ3DE$_{(15)}$ (0.5 μM) for 6 h in the presence of Lipofectin (5 μg/ml). After that time, the transfection mixture was replaced by normal serum-containing medium, and cells were grown for another 18 h. Attached, treated intact cells were maintained in a CO_2 incubator at 37 °C. Two control assays were carried out using either untreated cells or cells exposed to 0.25 μM fluorescein. After incubation, cells were washed three times with phosphate-buffered saline, fixed with freshly prepared 3.5% paraformaldehyde for 15 min at room temperature, washed three times with phosphate-buffered saline, mounted in 2.5% DABCO™ in glycerol, and processed for microscopy.

Fluorescence Spectroscopy—Fluorescence emission spectra were measured on an LS-50 spectrofluorometer (PerkinElmer Life Sciences), and spectra were corrected for lamp fluctuations and instrumental variations. Polarization artifacts were avoided by setting excitation and emission polarizers to magic angle conditions (54.74°). All of the fluorescence measurements were performed at the temperature of 23 ± 1 °C. Emission spectra, excitation spectra, and luminescence intensity were recorded with 5-nm band passes for both the excitation and emission monochromators. A cut-off filter in the emission beam was used to eliminate second-order wavelength interference. The excitation wavelengths used were 494 nm and 560 nm for fluorescein- and rhodamine-conjugated constructs, respectively. Emission spectra were corrected for the blank contribution and for the instrument response and normalized to the DNA concentration in a quartz cell with a 1-cm path length. Excitation and emission spectra were automatically corrected for lamp intensity variations. Buffers were degassed by bubbling nitrogen to prevent quenching of fluorescence by dissolved oxygen. The fluorescence emission signals were stable to photobleaching under the experimental conditions of measurement. The apparent interchromophore separation, *R*, the distance separating the energy donor and acceptor was calculated by the Forster equation: $r = R_0(1/E - 1)^{1/6}$, where *E* is the efficiency of energy transfer from donor to acceptor. $E = 1 - F_{DA}/F_D$ and R_0 is the distance for 50% transfer efficiency *E*. F_{DA} and F_D are the fluorescence intensities of the donor in the presence and absence of the acceptor, respectively. F_{DA} and F_D were measured at 520 nm, the emission maximum for fluorescein.

The fluorescence anisotropy of the fluorescein and rhodamine probes attached to the DNAzyme (Fluo-MeO-β3DE$_{(15)}$-Rhod, Fluo-MeO-β3DE$_{(11)}$-Rhod) was monitored in an LS-50 spectrofluorometer (PerkinElmer Life Sciences) equipped with an automatic anisotropy measuring device. The anisotropy *r* is defined as

$$r = (I_{VV} - G \times I_{VH}) / (I_{VV} + 2 \times G \times I_{VH}) \quad \text{(Eq. 1)}$$

where *I* is fluorescence intensity. The first and second indices refer to the orientation of excitation and emission polarizers, respectively. *G* is the correction factor. The cell holder was thermostated at 21 °C.

Analysis of Fluorescence Data—Efficiencies of energy transfer were determined from enhancement acceptor fluorescence (17, 18). The emission at a given wavelength (v1) of a double-labeled sample excited primarily at the donor wavelength (v′) contains emission from the donor, emission from directly excited acceptor, and emission from acceptor excited by energy transfer from the donor, *i.e.*

$$\begin{aligned} F(v_1,v') &= [S]\cdot\epsilon^D(v')\cdot\phi_D(v_1)\cdot d^+\cdot\{(1 - E_{FRET})\cdot a^+ + a^- \\ &\quad + \epsilon^A(v')\cdot\phi_A(v_1)\cdot a^+ + \epsilon^D(v')\cdot\phi_A(v_1)\cdot E_{FRET}\cdot d^+ + a^+\} \\ &= F^D(v_1,v') + F^A(v_1,v') \quad \text{(Eq. 2)} \end{aligned}$$

where [S] is the concentration of DNAzyme, d^+ and a^+ are the molar fraction of DNAzyme molecules labeled with donor and acceptor respectively, and a^- is the molar fraction of DNAzyme molecules unlabeled with acceptor. Superscripts D and A refer to donor and acceptor, respectively. $\epsilon^D(v')$ and $\epsilon^A(v')$ are the molar absorption coefficients of donor and acceptor, respectively, and $\phi_D(v_1)$ and $\phi_A(v_1)$ are the fluorescent quantum yields of donor and acceptor, respectively. Thus the spectrum contains the components due to donor emission [$F^D(v_1,v')$, *i.e.* the first term containing $\phi_D(v_1)$] and those due to acceptor emission [$F^A(v_1,v')$, *i.e.* the latter two terms containing $\phi_A(v_1)$]. The first stage of the analysis involves subtraction of the spectrum of DNA labeled only with donor, leaving just the acceptor components, *i.e.* $F^A(v_1,v')$. The pure acceptor spectrum thus derived is normalized to one from the same sample excited at a wavelength (v″) at which only the acceptor is excited, with emission at v^2. We then obtain the acceptor ratio

$$\begin{aligned} (\text{ratio})_A &= F^A(v_1,v') / F^A(v_2,v'') \\ &= \{E_{FRET}\cdot d^+\cdot[\epsilon^D(v') / \epsilon^A(v'') + \epsilon^A(v') / \epsilon^A(v'')]\}\cdot[\phi_A(v_1) / \phi_A(v_2)] \quad \text{(Eq. 3)} \end{aligned}$$

E_{FRET} is directly proportional to $(\text{ratio})_A$ and can be easily calculated because $\epsilon^D(v')/\epsilon^A(v'')$ and $\epsilon^A(v')/\epsilon^A(v'')$ are measured from absorption spectra, and $\phi_A(v_1)/\phi_A(v_2)$ is unity when $v_1 = v_2$.

Analysis of Circular Dichroism—The circular dichroism spectra of MeO-β3DE (1 μM), free or in the complex with the substrate (2 μM), was measured in a solution of 10 mM Tris-HCl, pH 7.5, containing increasing concentrations of $MgCl_2$ at 21 °C. In control experiments, 0.1 M and 1 M NaCl were used. Before measurement, the complex was allowed to form by heating the solution at 95 °C for 2.5 min followed by gradual cooling. Measurements were made in a quartz cuvette (5-mm path length) with a CD spectrometer (model CD6, Jobin Yvon) from 200 to 320 nm in triplicate. The spectra were obtained by smoothing the averaged spectra with a calculator.

Surface Plasmon Resonance—The kinetic parameters (association and dissociation rate constants, k_{on} and k_{off}, respectively) and the affinity constant (K_D) between DNAzyme and the mRNA substrate were measured by surface plasmon resonance using a BIAcoreX (Amersham Biosciences). Briefly, avidin was covalently attached to carboxymethyl dextran chips (CM5, BIAcore) previously activated with *N*-hydroxysuccinimide and *N*-ethyl-*N*′-dimethylaminopropyl carbodiimide, according to the manufacturer's instructions. Experiments were performed at 37 °C using 50 mM Tris, pH 8.0, containing divalent cations at the indicated concentrations. 15 μl of 5′ end-biotinylated RNA at 100 nM in 50 mM Tris, pH 8.0, was injected at the flow rate of 5 μl/min and

consequently immobilized on the bound avidin to give a response of ~500 resonance units, an arbitrary unit specific for the BIAcore instrument. The levels of immobilized RNA were within the low levels that have to be used to ensure that the observed binding rate will be limited by the reaction kinetics rather than by the mass transport effects of the injected DNAzyme (19). In typical experiments, DNAzyme flowed in two channels of the sensor; the first one contained the RNA substrate attached to avidin, and the second was without the RNA substrate. The latter was used to correct SPR traces and remove the background binding between DNAzyme and the immobilized avidin on the dextran. The concentration of the injected DNAzyme was in the range 20–200 nM, and the flow rate was 5 μl/min. The amount of ligand bound to immobilized RNA substrate was monitored by measuring the variation of the surface plasmon resonance angle as a function of time. Results were expressed in resonance units. In preliminary experiments, the data obtained for at least three different concentrations of DNAzymes were fitted to several models; the best fits ($\chi^2 = 1.4$) were obtained by assuming a one-to-one interaction. Then, the association rate constant, k_{on}, and dissociation rate constant, k_{off}, were determined separately from individual association and dissociation phases, respectively. The overall affinity constant, K_A, was derived from k_{on}/k_{off}. The sensor chip was regenerated with three 10-μl pulses of 12.5% formamide.

RESULTS

Enzymatic Characteristics of the DNAzyme to β3 Integrin Subunit—The 10–23 DNAzyme used in these studies was designed to cleave β3 integrin subunit mRNA, and preliminary characterization was done in our recent work (2). Standard conditions for kinetic measurements of the catalytic activity of DNAzyme *in vitro* include 25 mM $MgCl_2$ (20). Under such conditions, the 10–23 DNAzyme shows optimal enzymatic activity, whereas its mutant MeO-β3DE$_{(11)}$ with the shortened catalytic loop is inactive (Fig. 1*A*). In this experiment, enzymatic reactions were performed in 50 mM Tris-HCl, pH 8.0, containing 0–25 mM $MgCl_2$, under multiple turnover conditions. The ^{32}P-labeled mRNA substrate was mixed with the DNAzyme β3DE in the molar ratio of 80:1 and incubated at 37 °C; aliquots were withdrawn after 10 min. The cleavage reaction was stopped by the addition of 5 μl of 0.5 M EDTA, and products were separated by electrophoresis in 20% polyacrylamide gels under denaturing conditions. Amounts of the product were evaluated by use of a PhosphorImager. Fig. 1*B* shows a composition of cleavage mixtures obtained after a 60-min incubation of ^{32}P-labeled mRNA substrates with 0.025 μM β3DE added at a molar ratio ranging from 5:1 to 80:1. Each of the DNAzymes, unmodified (β3DE) and modified (MeO-β3DE), cleaved the substrate at the predicted site. Interestingly, DNAzyme with the 2′-MeO residues showed a significantly higher enzymatic activity than β3DE, as evidenced by the catalytic efficiency k_{cat}/K_m of 3.62×10^6 and 1.09×10^6 M^{-1} min^{-1}, respectively.

Study of Ion-induced Folding of the DNAzyme by Fluorescence Resonance Energy Transfer—To follow the folding transitions of the DNAzyme induced upon binding of Mg^{2+} ions, FRET was utilized. For this purpose, β3DE with the 15-mer and 11-mer catalytic loops was modified by attachment of the donor and acceptor fluorophores, rhodamine and fluorescein, to the 5′ and 3′ ends of the flanking arms, respectively. Next, a series of experiments were designed to analyze whether the fluorophores attached to the terminal bases affect the ability of the oligodeoxynucleotide construct to function as an active DNAzyme species. As seen in Fig. 2*A*, incubation of the Fluo-MeO-β3DE$_{(15)}$-Rhod with the ^{32}P-labeled substrate in the presence of 25 mM Mg^{2+} under multiple-turnover conditions at 37 °C leads to cleavage at the correct site. When such a construct was incubated with endothelial cells, it remained resistant to intracellular nucleases and, even after 24 h, was located exclusively within the cytoplasm, particularly in the perinuclear organelles. The cellular uptake, intracellular distribution, and stability of the Fluo-MeO-β3DE$_{(15)}$-Rhod were the same as those recently reported for another 10–23 DNAzyme (21). Cellular transport of the Fluo-MeO-β3DE$_{(15)}$-Rhod as a function of the external oligonucleotide concentration was nonlinear, being more efficient at concentrations below 2 μM. The punctate fluorescence distribution observed even after 24 h of exposure to the DNAzyme seems to suggest that endosomal vesicles are the primary targets of the probes under study (Fig. 2*B*). Fluo-MeO-β3DE$_{(15)}$-Rhod could be detected intracellularly, both when emission of either fluorescein or rhodamine was measured and both fluorophores showed full colocalization. Thus, the attached fluorophores did not influence the enzymatic activity and biological properties of the DNAzyme, including the ability to interact with cellular components responsible for its transport. Transfection of endothelial cells with the DNAzyme (5 μM) efficiently reduced expression of β3 integrin subunit measured at the level of β3 mRNA by reverse transcriptase-PCR (Fig. 2*C*) and at the cellular surface by flow cytometry (not shown). Although MeO-β3DE$_{(11)}$-Rhod had the same cellular distribution as MeO-β3DE$_{(15)}$-Rhod, it did not show any biological activity detectable at the level of β3 mRNA or β3 expression at the cell surface. These data provide the evidence that the 10–23 DNAzyme has an intracellular catalytic or antisense activity, even at the much lower cation concentrations than those normally used in *in vitro* analysis.

Both Fluo-MeO-β3DE$_{(15)}$-Rhod and Fluo-MeO-β3DE$_{(11)}$-Rhod were next used to measure energy transfer resulting from a dipolar coupling between the transition moments of the two fluorophores, fluorescein as the energy donor and rhodamine as the energy acceptor. When the fluorescence spectrum of one fluorophore (the donor) overlaps with the excitation spectrum of another fluorophore (the acceptor), the excitation of the donor induces fluorescence of the acceptor, although its own fluorescence decreases. The extent of FRET is extremely sensitive to the distance between the donor and the acceptor, being inversely proportional to the sixth power of the distance. Attachment of rhodamine to Fluo-MeO-β3DE$_{(15)}$ resulted in a decrease in the fluorescence emission at 520 nm characteristic for fluorescein, and the fluorescence spectrum of the resulting construct, Fluo-MeO-β3DE$_{(15)}$-Rhod, had two peaks at 520 nm and 580 nm upon excitation at 494 nm (Fig. 3). The mutated β3DE, Fluo-MeO-β3DE$_{(11)}$-Rhod, showed the same fluorescence properties. These spectra clearly indicate that considerable energy from the excited fluorescein was transferred to rhodamine, providing the evidence that both fluorophores are in close proximity. Cleavage of the Fluo-MeO-β3DE$_{(15)}$-Rhod with endonuclease from *Serratia marcescens* resulted in a significant increase of the fluorescence intensity at 520 nm, which approaches the level of fluorescein alone, indicating that both fluorophores are separated to the distance enabling the energy transfer.

Variation in End-to-end Distances during the Ion-induced Folding of the DNAzyme—According to the model for the folding of the DNAzyme, the length of oligodeoxynucleotide should shorten over the full range of Mg^{2+} concentration. Experimentally, we find that E_{FRET} increases rapidly upon the addition of cations to Fluo-MeO-β3DE$_{(15)}$-Rhod and reaches a plateau value by 5 mM Mg^{2+}. Assuming a Forster critical distance (R_0) of 5.5 nm for donor-fluorescein (22), the distance between donor (fluorescein) and acceptor (rhodamine) in the absence of Mg^{2+} was calculated to be 7.82 + 0.39 nm and was not significantly dependent upon the DNAzyme concentration. The distance between two fluorophores shortens over this range from 7.82 nm to 6.22 nm and further addition of Mg^{2+} ions does not essentially change it (Fig. 4*A*). At 25 mM Mg^{2+}, the R value reaches 6.11 nm and is almost identical to that characteristic for the Fluo-MeO-β3DE-Rhod in the complex with its mRNA

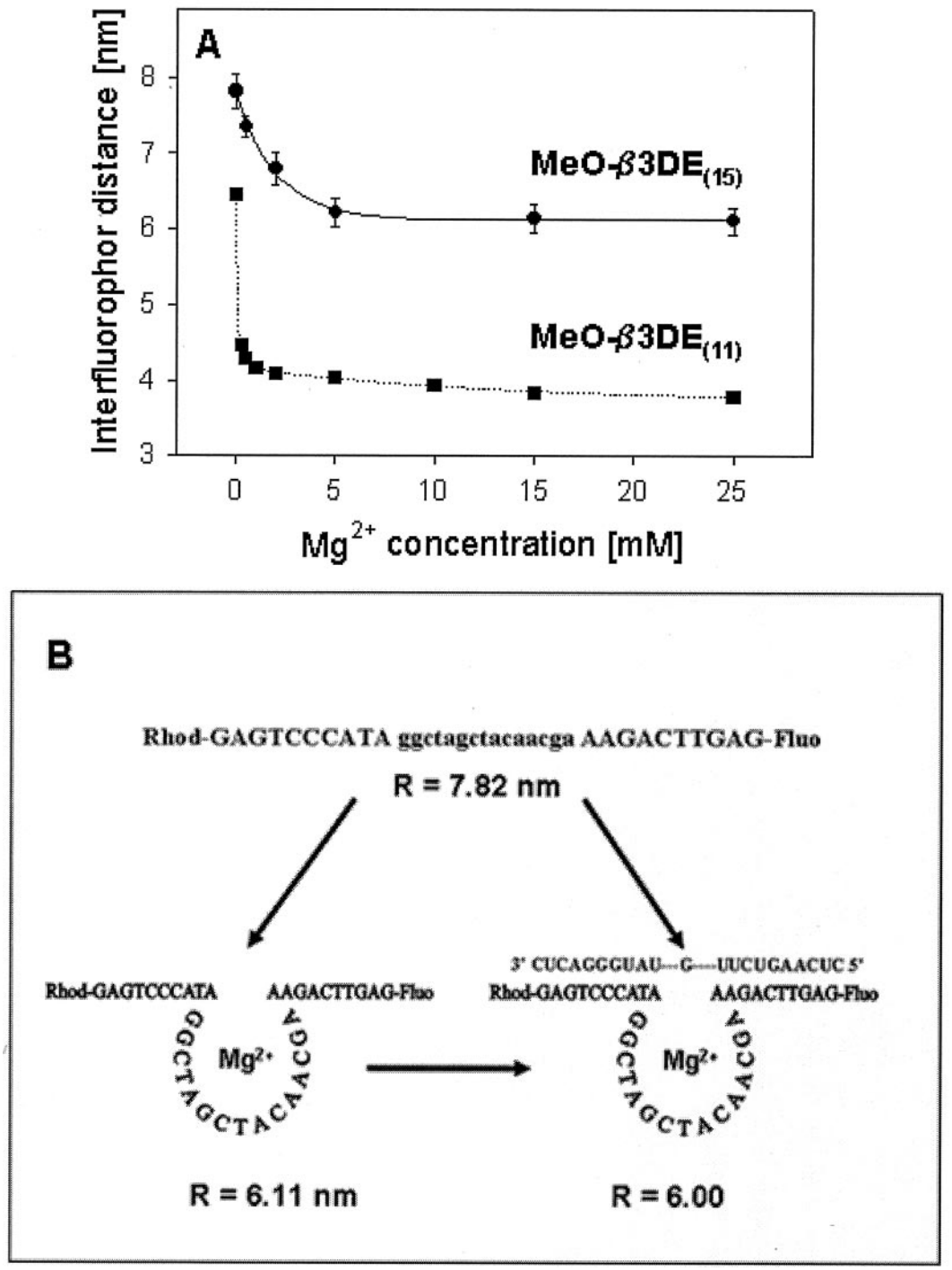

FIG. 4. **FRET analysis for the MeO-β3DE as a function of Mg^{2+} concentration.** *A*, calculated interfluorophore distances based on measured efficiency of energy transfer presented as a function of $MgCl_2$ concentration. The plot shows the variation in FRET efficiency as a function of Mg^{2+} concentration up to 25 mM when Fluo-MeO-β3$DE_{(15)}$-Rhod (●–●) or Fluo-MeO-β3$DE_{(11)}$-Rhod (■–■) were tested. In accordance with the model, the FRET efficiency is found to increase (indicating a reducing end-to-end distance) over this complete range. *B*, scheme with the expected behavior of the free DNAzyme or complexed with its RNA substrate in the presence of Mg^{2+}. The distances (*R*) were calculated based on FRET analysis.

substrate. Essentially the same changes in the interfluorophore distance were induced in the Fluo-MeO-β3DE-Rhod upon binding of other divalent cations, such as Ca^{2+} and Mn^{2+} (Table I). Such folding of the DNAzyme does not result simply from the neutralization of the polyanionic nature of the oligodeoxynucleotide, because neither Na^+ nor K^+ added in place of Mg^{2+}, even at 1 M, showed any effect. In the case of DNAzyme with the 11-mer loop, Fluo-MeO-β3$DE_{(11)}$-Rhod, E_{FRET} dramatically increased upon the addition of 0.5 mM Mg^{2+}, indicating that these cations induce folding of the mutated deoxyribozyme by means of high affinity binding to sites (Fig. 4*B*).

To evaluate overall changes induced in the DNAzyme by cations, the fluorescence anisotropy of both fluorophores in Fluo-MeO-β3DE-Rhod was measured in the presence of increasing concentrations of Mg^{2+}, Ca^{2+}, Li^+, Na^+, and K^+. The fluorescence anisotropy *r* reflects the local and global motions of the fluorophore and is close to zero for a freely rotating fluorophore. The theoretical upper limit of 0.4 corresponds to a totally non-rotating fluorophore (23). The fluorescein- and rhodamine-labeled DNAzyme has a flexible single-stranded mole-

cule characterized by a low r value = 0.016 and 0.037, as measured for fluorescein and rhodamine, respectively (Fig. 5). In both cases, the fluorescence anisotropy doubles when Mg^{2+} or Ca^{2+} concentration reached 5 mM or 1 mM, respectively, indicating the increased condensation state of the molecule. However, there was no change in the fluorescence anisotropy when monovalent cations were used even at much higher concentrations (Fig. 5). These results are fully consistent with the proposed mechanism involving the divalent cation-induced folding of the DNAzyme and indicate that its molecule becomes more compact upon Mg^{2+} binding.

TABLE I
The estimated interfluorophore distance based on FRET analysis of the Fluo-MeO-β3 DE-Rhod

The fluorophore-labeled MeO-β3DE (40 nM) was incubated with different divalent cations used in the concentration range from 0 to 25 mM, and the interfluorophore distance R was evaluated based upon the Forster equation. Data represent a mean value of three separate determinations.

Concentration	Interfluorophore distance [nM]		
	Mg^{2+}	Ca^{2+}	Mn^{2+}
mM			
0	7.823	8.040	8.165
5	6.215	6.237	6.167
15	6.143	6.087	6.099
25	6.107	6.042	6.059

Complex Formation between DNAzyme and its RNA Substrate—The conformational changes of the DNAzyme induced by Mg^{2+} were next analyzed by CD spectroscopy (Fig. 6). CD spectra of an ion-free DNAzyme/RNA complex were reported earlier (24). We have been interested in examining how far CD spectroscopy (being sensitive to the structure helicity and fold) could be applicable to probing binding of metal ions to single- and double-stranded species of interest. As the reference, CD spectra related to a regular complex formation (Fig. 6*A*), reflecting an antisense mechanism, were inspected first. The CD

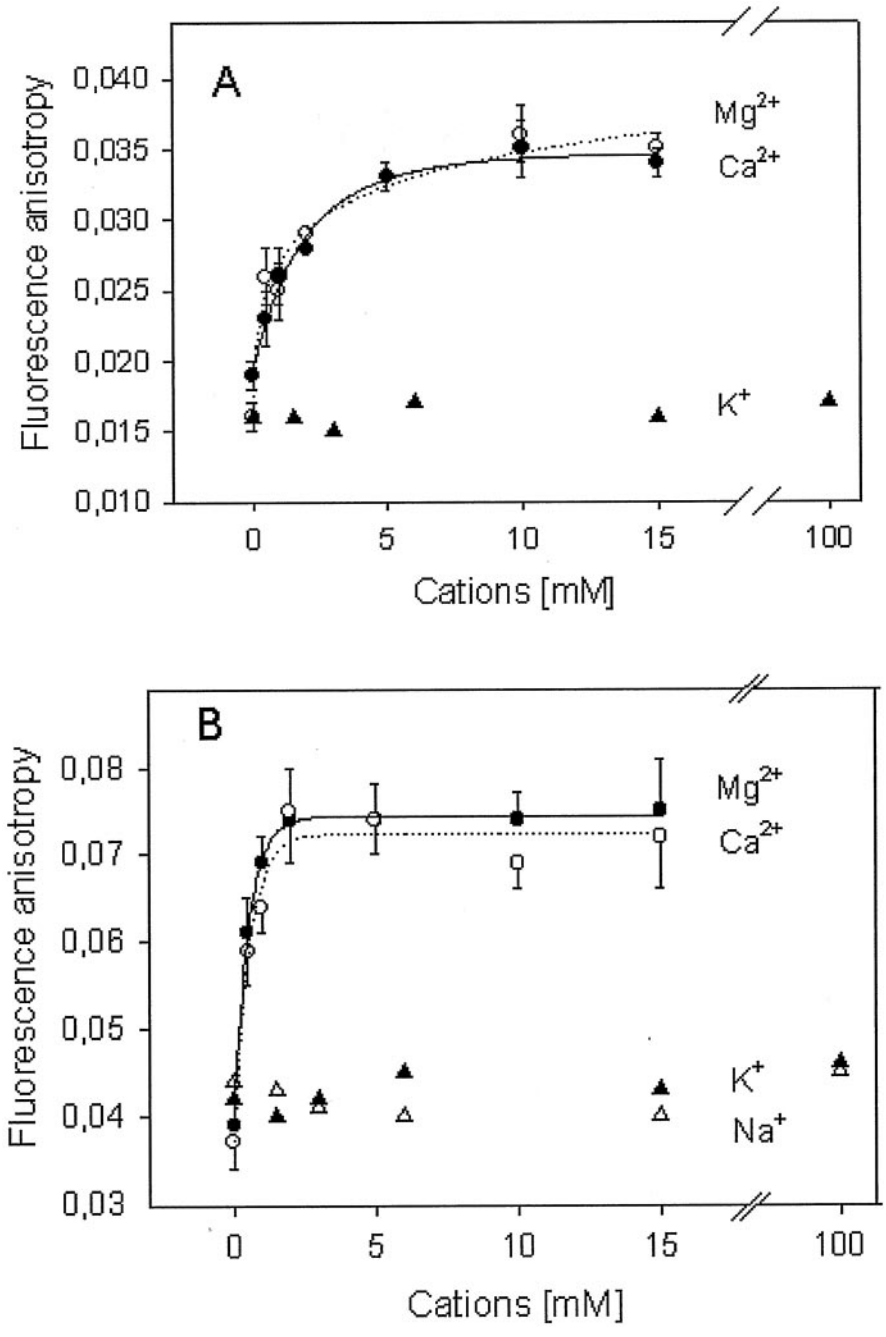

FIG. 5. **Effect of Mg^{2+} on the fluorescence anisotropy of Fluo-MeO-β3DE-Rhod.** $MgCl_2$ (●–●), $CaCl_2$ (○–○), KCl (▲–▲), and NaCl (△–△) were added stepwise to 0.5 μM Fluo-MeO-$β3DE_{(15)}$-Rhod and incubated for 5 min before measuring the fluorescence anisotropy. To monitor the fluorescence anisotropy of fluorescein (*A*) or rhodamine (*B*), the samples were excited at 494 nm or 560 nm and fluorescence emission was measured at 520 nm or 580 nm, respectively.

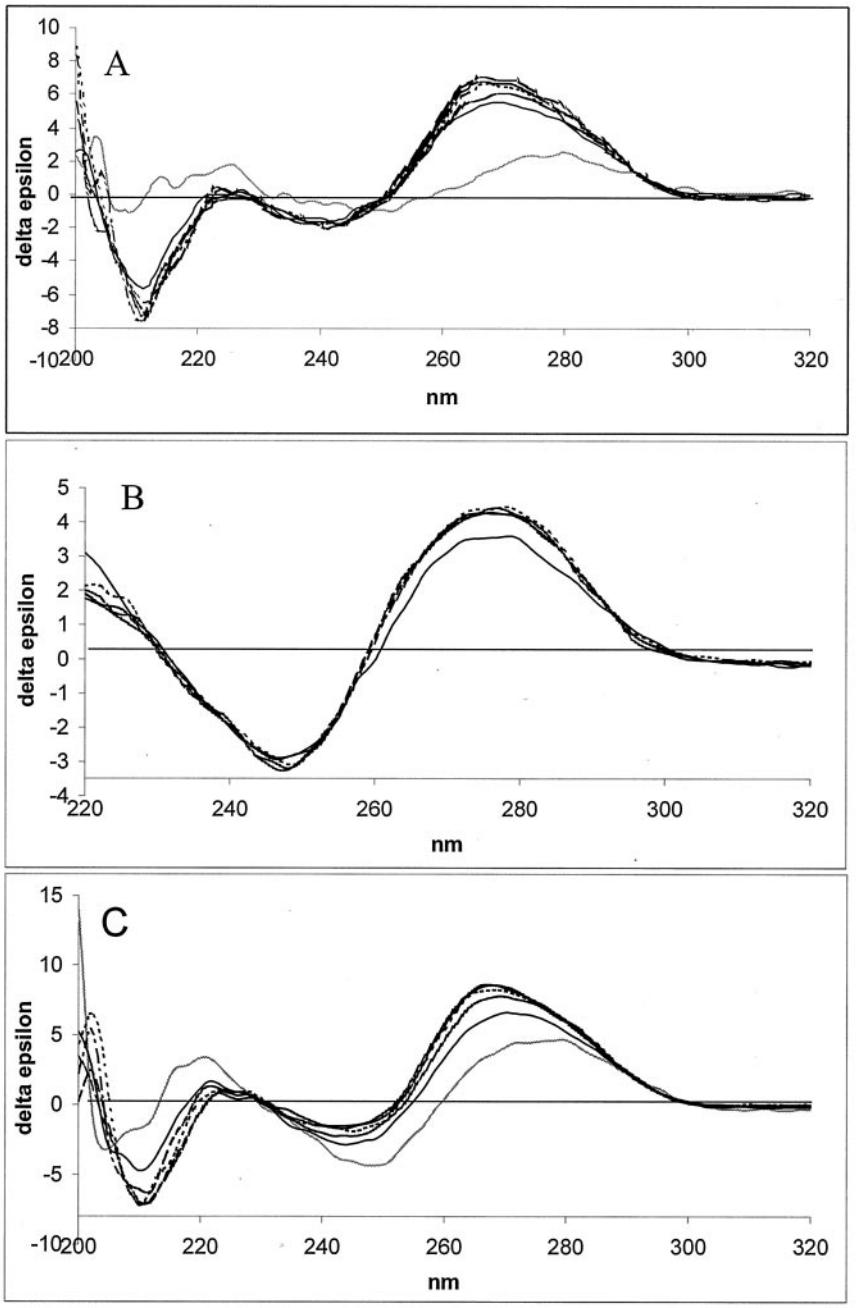

FIG. 6. **Effect of Mg^{2+} on CD spectra of the free MeO-β3DE and its complex with the target RNA.** CD spectra of the antisense oligodeoxynucleotide MeO-β3(1245–1265)/RNA complex (*A*), the single stranded MeO-β3DE (*B*), and the MeO-β3DE/RNA complex (*C*) were taken in the presence of Mg^{2+} concentrations ranging from 0 to 25 mM. However, because there was no change when concentrations higher than 5 mM Mg^{2+} were used, those spectra were deleted for clarity of the plot. Spectra of the single-stranded antisense oligodeoxynucleotide MeO-β3(1245–1265) and MeO-β3DE are shown as a *gray line* in *A* and *C*, respectively. Spectra were taken at the following Mg^{2+} concentrations: 0 mM (—), 0.5 mM (----), 1.0 mM (· · · ·), 2.0 mM (-· -· -· -·), and 5.0 mM (-· · -· · -·).

spectrum of a non-enzymatic, single 21-mer DNA strand is irregular and of low magnitude. Addition of a complementary RNA strand resulted in raising a regular positive Cotton effect at 269 nm, *i.e.* a region typical of the DNA/RNA hybrids (25). Influence of an increased Mg^{2+} concentration on a double helical structure is not strong but clearly visible, as indicated by the increase in amplitude of the Cotton effect. An initial addition of Mg^{2+} (0.5 mM) resulted in both a higher Cotton effect than that produced by 1 mM Mg^{2+} and the formation of two characteristic, discrete peaks (265 nm and 269 nm). At concentrations higher than 1 mM Mg^{2+}, the height of these peaks is reversed and kept practically unchanged, even at higher Mg^{2+} concentrations of up to 25 mM. The positive CD band of the Mg^{2+}-free DNAzyme, although rather broad (276–278 nm), is much more regular (Fig. 6*B*) than that of the 21-mer oligodeoxynucleotide. The spectrum also contains a negative effect at 249 nm and a weak, positive effect at 221 nm. This result indicates that some secondary structure exists for the 35-mer strand of MeO-β3DE, most probably close to that predicted by the DNA-folding algorithm (26). An addition of Mg^{2+} at the initial concentration level (0.5 mM) led to a formation of a more regular and higher amplitude positive band at 276 nm. Further Mg^{2+} additions (up to 25 mM) had no practical effect on the DNAzyme strand spectra. The binding of the Mg^{2+}-free MeO-β3DE strand to the target RNA leads to the formation of a new type of spectrum with a positive Cotton band at 270 nm of higher amplitude than that of the DNAzyme strand (Fig. 6*C*). Both the lack of the symmetry for this band and the appearance of the weaker negative effect at 244 nm and positive effect at 223 nm are characteristic for the spectrum. Upon addition of an initial amount of Mg^{2+} (0.5 mM), the amplitude of the positive Cotton effect rises substantially, and the peak is shifted down to 268 nm. No further increase of the Cotton effect was observed above 1 mM Mg^{2+}. The results presented above indicate that, upon binding of Mg^{2+}, the global geometry of the DNAzyme adopts a compact structure projecting flanking arms

TABLE II

Kinetic parameters for binding of β3DE or antisense oligodeoxynucleotide β3(1245-1265) to immobilized RNA substrate and their dependence upon Mg^{2+} concentration

The 3′ end biotinylated RNA substrate (GUUCCACUCGUUAUCUUC) was immobilized on a BIAcore™ CM5 sensor chip coated with avidin (ΔRU = 5000). The analyte was injected at a flow of 5 μl/min, and measurements were done at 37 °C using 50 mM Tris, pH 8.0, containing divalent cations at the indicated concentrations. MeO-β3DE used in these experiments was inactive due to a single base substitution ($G^6 \rightarrow A$). The interaction of the corresponding oligodeoxynucleotide β3(1245-1265) containing both flanking arms of the β3DE with the same RNA substrate was analyzed under the same conditions. This oligodeoxynucleotide was modified as in MeO-β3DE. The k_{on} and k_{off} were determined from the association and dissociation phases, respectively, with four different concentrations of the DNAzyme and the oligodeoxynucleotide. Apparent K_A corresponds to k_{on}/k_{off} ratio. Data are shown as a mean value of four separate analyses.

DNA	Mg^{2+}	Ca^{2+}	k_{on} (1/Ms)	k_{off} (1/s)	K_A (1/M)
	mM	*mM*			
β3DE	5.0		$(8.23 \pm 0.53) \times 10^4$	$(1.98 \pm 0.94) \times 10^{-3}$	$(2.25 \pm 0.43) \times 10^7$
	15.0		$(8.47 \pm 0.77) \times 10^4$	$(2.99 \pm 1.05) \times 10^{-3}$	$(3.16 \pm 1.23) \times 10^7$
	25.0		$(1.23 \pm 0.28) \times 10^5$	$(2.84 \pm 1.53) \times 10^{-3}$	$(6.91 \pm 2.60) \times 10^7$
		5.0	$1.20 \pm 0.11) \times 10^5$	$3.22 \pm 0.94) \times 10^{-3}$	$2.74 \pm 0.84) \times 10^7$
		15.0	$9.51 \pm 0.15) \times 10^4$	$3.09 \pm 0.86) \times 10^{-3}$	$3.05 \pm 1.01) \times 10^7$
		25.0	$8.55 \pm 0.79) \times 10^4$	$2.84 \pm 0.94) \times 10^{-3}$	$5.71 \pm 2.71) \times 10^7$
β3(1245-1265)	5.0		$(3.44 \pm 1.04) \times 10^4$	$(1.41 \pm 0.49) \times 10^{-4}$	$(1.64 \pm 0.29) \times 10^8$
	15.0		$(6.04 \pm 2.10) \times 10^4$	$(3.76 \pm 0.53) \times 10^{-4}$	$(1.78 \pm 0.88) \times 10^8$
	25.0		$(8.49 \pm 2.15) \times 10^4$	$(5.90 \pm 0.18) \times 10^{-4}$	$(1.46 \pm 0.40) \times 10^8$
		5.0	$5.22 \pm 1.46) \times 10^4$	$8.40 \pm 1.88) \times 10^{-4}$	$1.19 \pm 0.84) \times 10^8$
		15.0	$7.84 \pm 1.48) \times 10^4$	$6.11 \pm 1.02) \times 10^{-4}$	$1.37 \pm 0.52) \times 10^8$
		25.0	$9.41 \pm 2.94) \times 10^4$	$7.21 \pm 1.50) \times 10^{-4}$	$1.48 \pm 0.83) \times 10^8$

at right position and angles to bind substrate mRNA.

To further test this concept, the binding kinetics were directly measured by surface plasmon resonance analysis in the presence of increasing concentrations of Mg^{2+}. In these experiments, biotinylated RNA substrate was attached to the avidin-coated sensor. To avoid cleavage of the RNA substrate, the inactive DNAzyme containing a single nucleotide substitution in the catalytic domain of β3DE was used. The antisense oligodeoxynucleotide β3(1245–1265) consisting of both flanking arms (and thus antisense to β3 integrin subunit mRNA) was tested as a control. To clarify the effect of cations on association and dissociation processes between the DNAzyme and its RNA substrate, we determined the parameters of k_{on}, k_{off}, and K_A in the binding reactions between RNA substrate and either DNAzyme or the antisense oligodeoxynucleotide (Table II). The binding affinity of β3 DNAzyme to the RNA substrate was dependent upon the concentration of Mg^{2+}. The association constant determined in the presence of 15 mM Mg^{2+} was significantly higher ($p < 0.001$) than that observed at 5 mM of Mg^{2+}. However, it was still much lower than the K_A describing the interaction of the antisense oligodeoxynucleotide with the same RNA fragment. Interestingly, the binding affinity of the antisense oligodeoxynucleotide to the RNA substrate did not depend upon cation concentration, and regardless of the Mg^{2+} presence, it was almost an order of magnitude higher than that of the DNAzyme.

DISCUSSION

The intracellular ability of various 10–23 DNAzymes to inhibit expression of the targeted proteins was evidenced by several *in vitro* and *in vivo* studies (27), indicating their potential advantages as biocatalysts in oligonucleotide therapy. Despite tremendous therapeutic potential, the ability of the DNAzyme to influence biological processes has not been determined at the molecular level. Because of its high flexibility, the three-dimensional structure of the DNAzyme molecule is not yet known. Therefore, even a basic knowledge about the mechanism by which Mg^{2+} and other divalent cations regulate enzymatic activity of the 10–23 DNAzyme is at present speculative. The hypothetical mechanism for catalysis of RNA cleavage by the DNAzyme is essentially based on assumptions that it behaves similarly to the hammerhead ribozyme, which also is active in the presence of various divalent metal cations (28). Despite different compositions, the 10–23 DNAzyme and the hammerhead ribozyme show many common features, including the divalent cation dependence and kinetic parameters of RNA cleavage. Exhaustive studies on chimeric DNAzymes and substrates composed of DNA and RNA showed that both types of enzymes have a very similar catalytic mechanism (5). The reactions have an identical dependence on pH, both demonstrate an inverse correlation between the pK_a of metal hydrates and activity and solvent isotope effects, and thio effects on the reactions are identical (24). The crystal structure of several unmodified and modified hammerhead RNA in the absence of divalent metal ions has been solved (28, 30–32). Cation binding sites and the mechanism by which they control enzymatic activity have been elucidated (30, 33). Five Mg^{2+} sites are seen in the crystal structure of the Mg^{2+}-soaked freeze-trapped conformational intermediate of the hammerhead ribozyme, which could be divided into two groups based on their roles in catalytic activity. The first group consists of Mg^{2+} sites that upon binding of cations induce folding of the enzyme into its active conformation. The second group includes sites occupied by Mg^{2+} bound directly to the optically active oxygen showing R diastereomeric form (pro-R) at the cleavage site. The hammerhead ribozyme can cleave its own RNA, and this activity requires one or more catalytic divalent metal ions, one of which ionizes the 2′-hydroxyl at the cleavage site. The newly generated nucleophile attacks the adjacent phosphate by an in-line mechanism. The same metal ion, or perhaps another, stabilizes the pentacoordinated phosphate transition state by binding directly to the pro-R phosphate oxygen. The reaction generates 5′-hydroxyl and 2′,3′-cyclic phosphate termini at the cleavage site (34).

The structural effect of Mg^{2+} is well established in the hammerhead ribozyme (35). In the absence of divalent metal ions, the hammerhead structure is extended, with a disordered core, but upon addition of metal ions, folding occurs in two distinct steps. Both events are well described by two-state transitions induced by the non-cooperative binding of Mg^{2+}. One can assume that similarly to the hammerhead ribozyme, metal ions will induce the folding of the DNAzyme molecule into the geometry required to facilitate the pathway into the transition state and will also bind at a specific location(s), where they can participate directly in the chemistry of the cleavage reaction.

Data presented in this report show that binding of Mg^{2+} to the 10–23 DNAzyme induces significant rearrangement of the catalytic loop, which leads to optimal folding of the molecule. This folding may occur in several distinct stages. The first

transition induced by 0.5 mM Mg^{2+} results in the formation of a compact structure of the DNAzyme. The DNAzyme in such a state binds weakly to its RNA substrate and lacks catalytic activity. In the next stage observed at concentrations up to 5 mM Mg^{2+}, the flanking arms are projected into the proper position to bind the RNA substrate. Under such conditions, the DNAzyme binds efficiently to the substrate and shows substantial catalytic activity. Further increase of Mg^{2+} leads to the final transition, involving formation of the completely organized catalytic domain of the DNAzyme. Such a mechanism is supported by the following observations: (i) E_{FRET} of the Flu-MeO-β3DE$_{(15)}$-Rhod rapidly increases in the range from 0 to 5 mM cations and reaches a plateau value by 5 mM Mg^{2+}, indicating at this concentration the shortest distance between the energy donor and acceptor. In the absence of Mg^{2+}, the DNAzyme is inactive and its catalytic core is essentially unfolded. With the addition of 5 mM Mg^{2+}, the orientation of the catalytic loop changes, and the distance between 5′ and 3′ ends almost reaches the value characteristic for the DNAzyme in complex with its RNA substrate. Under these conditions, the DNAzyme shows substantial enzymatic activity. A significant increase in the catalytic activity of the DNAzyme is observed when the Mg^{2+} concentration is increased from 5 to 15 mM, suggesting that additional structural alterations within the catalytic loop have occurred, even though there was no further change in E_{FRET}. The hyperbolic concentration dependence of the end-to-end distance with a midpoint of ~2 mM Mg^{2+}, which is significantly lower than that characteristic for the chemical cleavage step (Fig. 2), indicates that structural changes induced in the DNAzyme occur at much lower Mg^{2+} concentrations than those required for the catalytic properties. This conclusion is supported by the observation that the mutated inactive variant of the MeO-β3DE, with the shortened catalytic loop, adopts the compact structure at a much lower Mg^{2+} concentration, indicating that such a structural transition is not sufficient to gain catalytic activity. (ii) The fluorescence anisotropy of Flu-MeO-β3DE-Rhod doubles after exposure to the increasing concentrations of Mg^{2+} or Ca^{2+} and reaches the maximum at their concentration of 1–5 mM, indicating the increased condensation state of the molecule under these conditions. (iii) Saturation effects of Mg^{2+} concentrations detected by CD spectroscopy were produced in the range from 0.5 to 2.0 mM, *i.e.* somewhat lower than that described by other techniques. As expected, spectra of the DNA/RNA hybrid (positive effect at 269 nm), used as a referenced structure close to a regular A-type helix (36, 37), were much less sensitive to Mg^{2+} than those of the DNAzyme strand and its complex with RNA. The Mg^{2+}-free MeO-β3DE strand (effect at 276–278 nm) undergoes a considerable change both upon Mg^{2+} binding (276 nm) and further structural stabilization upon binding to the target RNA strand. It should be emphasized that these conformational changes take place at a Mg^{2+} concentration as low as 0.5 mM. An overall similarity of the DNAzyme/RNA complex spectra (Fig. 6*C*) to that typical for A-type RNA/DNA hybrids was observed (25). This finding also confirms an earlier observation based upon various Mg^{2+}-free DNAzyme complexes that the hybrid nature of the flanking arms strongly influences their global geometry (24). (iv) The final form adopted at 15 mM Mg^{2+}, showing high binding affinity toward the mRNA substrate, is in good agreement with the global form of the structure observed under the same conditions for the hammerhead ribozyme (29, 30, 38). Interestingly, the binding affinity of the DNAzyme to RNA increased linearly in the presence of divalent cations when they were used in the range from 0 to 15 mM, but it was still much lower than that of the antisense oligodeoxynucleotide consisting of the DNAzyme flanking arms. (v) Essentially the same effect on the folding, binding affinity to RNA substrate and catalytic activity of the DNAzyme were found when other divalent cations such as Ca^{2+} and Mn^{2+} were used in the same concentration range. Monovalent cations such as Na^{+}, K^{+}, and Li^{+} added in place of Mg^{2+} even at much higher concentrations of up to 1 M did not show any effect.

Acknowledgments—We thank Dr. A. Okruszek for synthesis of oligodeoxynucleotides and Dr. M. Koziolkiewicz for stimulating discussions.

REFERENCES

1. Santoro, S. W., and Joyce, G. F. (1997) *Proc. Natl. Acad. Sci. U. S. A.* **94,** 4262–4266
2. Cieslak, M., Niewiarowska, J., Nawrot, M., Koziolkiewicz, M., Stec, W. J., and Cierniewski, C. S. (2002) *J. Biol. Chem.* **277,** 6779–6787
3. Liu, C., Cheng, R., Sun, L. Q., and Tien, P. (2001) *Biochem. Biophys. Res. Commun.* **284,** 1077–1082
4. Zhang, L., Gasper, W. J., Stass, S. A., Ioffe, O. B., Davis, M. A., and Mixson, A. J. (2002) *Cancer Res.* **62,** 5463–5469
5. He, Q. C., Zhou, J. M., Zhou, D. M., Nakamatsu, Y., Baba, T., and Taira, K. (2002) *Biomacromolecules* **3,** 69–83
6. Santoro, S. W., and Joyce, G. F. (1998) *Biochemistry* **37,** 13330–13342
7. Chiu, T. K., and Dickerson, R. E. (2000) *J. Mol. Biol.* **25,** 915–945
8. Welche, J. B., Duckett, D. R., and Lilley, D. M. (1993) *Nucleic Acids Res.* **21,** 4548–4555
9. Soyfer, V. N., and Potaman, V. N. (1966) *Triple-helical Nucleic Acids*, p. 360, Springer, New York
10. Brukner, I., Susic, S., Dlakic, M., Savic, A., and Pongor, S. (1994) *J. Mol. Biol.* **11,** 26–32
11. Dahlgreen, P. R., and Lyubchenko, Y. L. (2002) *Biochemistry* **41,** 11372–11378
12. Scott, W., and Klug, A. (1996) *Trends Biochem. Sci.* **21,** 220–224
13. Cierniewski, C. S., Babinska, A., Swiatkowska, M., Wilczynska, M., Okruszek, A., and Stec, W. (1995) *Eur. J. Biochem.* **227,** 494–499
14. Okumoto, Y., and Sugimoto, N. (2000) *J. Inorg. Chem.* **82,** 189–195
15. Jaffe, E. A., Minich, R., Adelman, B., Becker, C. G., and Nachman, R. L. (1976) *J. Exp. Med.* **144,** 209–221
16. Jaffe, E. A., Nachman, R. L., Becher, C. G., and Minich, C. R. (1973) J. *Clin. Invest.* **52,** 2745–2756
17. Clegg, R. M. (1992) *Methods Enzymol.* **211,** 353–388
18. Clegg, R. M., Murchie, A. I. H., Zechel, A., and Lilley, D. M. J. (1993) (1993) *Proc. Natl. Acad. Sci. U. S. A.* **90,** 2994–2998
19. Bondeson, K., Frostell-Karlsson, A., Fagerstam, L., and Magnusson, G. (1993) *Anal. Biochem.* **214,** 245–251
20. Kumar, P. K. R., Zhou, D.-M., Yoshinari, K., and Taira, K. (1996) in *Catalytic RNA, Nucleic Acids and Molecular Biology* (Eckstein, F., and Lilley, D. M. J., eds) Vol. 10, pp. 217–230, Springer-Verlag, Berlin
21. Dass, C. R., Saravolac, E. G., Li, Y., and Sun, L. Q. (2002) *Antisense Nucleic Acid Drug Dev.* **12,** 289–299
22. Zhou, D.-M., Usman, N., Wincott, F. E., Matulic-Adamic, J., Orita, M., Zhang, L.-H., Komiyama, M., Kumar, P. K. R., and Taira, K. (1996) J. *Am. Chem. Soc.* **118,** 5862–5866
23. Lakowicz, J. R. (1983) *Principles of Fluorescence Spectroscopy*, Plenum Press, New York
24. Ota, N., Warashina, M., Hirano, K., Hatanaka, K., and Taira, K. (1998) *Nucleic Acids Res.* **26,** 3385–3391
25. Clark, C. L., Cecil, P. K., Singh, D., and Gray, D. M. (1997) *Nucleic Acids Res.* **25,** 4098–4105
26. Zuker, M. (2003) *Nucleic Acids Res.* **31,** 1–10
27. Khachigian, L. M. (2002) *Curr. Opin. Mol. Ther.* **4,** 119–121
28. Dahm, S. C., and Uhlenback, O. C. (1991) *Biochemistry* **30,** 9464–9469
29. Pley, H. W., Flaherty, K. M., and McKay, D. B. (1994) *Nature*, **372,** 68–74
30. Pley, H. W., Flaherty, K. M., and McKay, D. B. (1994) *Nature* **372,** 111–113
31. Scott, W. G., Finch, J. T., and Klug, A. (1995) *Cell* **81,** 991–1002
32. Ruffner, D. E., Stormo, G. D., and Uhlenbeck, O. C. (1990) *Biochemistry* **29,** 10695–10702
33. McKay, D. B. (1996) *RNA* **2,** 395–403
34. Scott, W. G., Murray, J. B., Arnold, J. R. P., Stoddard, B. L., and Klug, A. (1996) *Science* **274,** 2065–2069
35. Bassi, G. S., Murchie, A. I., Walter, F., Clegg, R. M., and Lilley, D. M. (1997) *EMBO J.* **16,** 7481–7489
36. Moore, D. S., and Wagner, T. E. (1974) *Biopolymers*, **13,** 977–986
37. Fairall, L., Martin, S., and Rhodes, D. (1989) *EMBO J.*, **8,** 1809–1817
38. Breaker, R. R., and Joyce, G. F. (1995) *Chem. Biol.* **2,** 655–660